





## Orbital angular momentum dynamics of Bose-Einstein condensates trapped in two stacked rings

Eulàlia Nicolau <sup>1,\*</sup>, Jordi Mompart <sup>1</sup>, Bruno Julià-Díaz <sup>2,3</sup> and Verònica Ahufinger <sup>1</sup>

<sup>1</sup>*Departament de Física, Universitat Autònoma de Barcelona, E-08193 Bellaterra, Spain*

<sup>2</sup>*Departament de Física Quàntica i Astrofísica, Facultat de Física, Universitat de Barcelona, 08028 Barcelona, Spain*

<sup>3</sup>*Institut de Ciències del Cosmos, Universitat de Barcelona, ICCUB, Martí i Franquès 1, 08028 Barcelona, Spain*



(Received 17 January 2020; accepted 9 July 2020; published 27 August 2020)

We investigate the stability and dynamics of the orbital angular momentum modes of a repulsive Bose-Einstein condensate trapped in two tunnel-coupled rings in a stack configuration. Within mean-field theory, we derive a two-state model for the system in the case in which we populate both rings equally with a single orbital angular momentum mode and include small perturbations in other modes. Analyzing the fixed-point solutions of the model and the associated classical Hamiltonian, we characterize the destabilization of the stationary states and the subsequent dynamics. By populating a single orbital angular momentum mode with an arbitrary population imbalance between the rings, we derive analytically the boundary between the regimes of Josephson oscillations and macroscopic quantum self-trapping and study numerically the stability of these solutions.

DOI: [10.1103/PhysRevA.102.023331](https://doi.org/10.1103/PhysRevA.102.023331)

### I. INTRODUCTION

Ultracold atoms trapped in ring potentials are one of the most promising systems in the emerging field of atomtronics [1,2]. They have been considered for quantum sensing applications such as rotation sensing [3,4], magnetometry [5], Sagnac interferometry [6–11], and the atomic analog to superconducting quantum interference devices (SQUIDs) [12–20]. Rings are the simplest geometries that lead to nontrivial loop circuits, in which the superfluidity of Bose-Einstein condensates (BECs) gives rise to persistent currents [21,22]. One can transfer orbital angular momentum (OAM) to the trapped BEC either by rotation of a weak link [13] or by coherent transfer of angular momentum from the photons to the atoms [23]. Regarding the implementation of the ring trapping potential, several techniques have been implemented or proposed: magnetic traps [24–26], conical refraction [27], pairs of optical fibers [28], static Laguerre-Gauss Beams [29], and time-averaged [3,4,30] or painting [31,32] potentials.

On the other hand, the Josephson effect is a fundamental phenomenon in quantum mechanics that has been widely explored in superconductors, and its study has recently been extended to bosonic ultracold atomic systems [33–38]. Josephson oscillations can arise in weakly coupled BECs trapped in a double-well potential: when there is a nonzero population imbalance, quantum tunneling allows the particles to oscillate periodically from one well to the other. However, repulsive interactions can suppress tunneling such that the atoms remain mostly trapped in one of the wells, a regime known as macroscopic quantum self-trapping [35]. Weakly coupled condensates have been proposed as basic building blocks for quantum technologies [39–42]. In particular, the dynamics of BECs in tunnel-coupled ring potentials have been

thoroughly explored in a variety of geometries such as stacked rings with [43,44] or without [45–53] lattices, concentric rings [54,55], and coplanar rings [56,57].

In this work, we investigate a BEC trapped in two rings in a stack configuration to study the interplay between the OAM, the tunneling dynamics, and the repulsive nonlinear interactions. First, we consider an initial state with a single OAM mode equally populated in both rings, which gives rise to symmetric and antisymmetric stationary states. The stability conditions of these states against OAM perturbations were derived within the mean-field theory and using Bogoliubov analysis in [46]. Here, we revisit the problem and demonstrate that the system can be described by a two-state model with fixed-point solutions. In particular, one can derive a classical Hamiltonian that characterizes the dynamics of the system in terms of the orbits around the critical points. Second, we consider an initial state where a single OAM mode is populated with a nonzero population imbalance between rings, such that tunneling and interactions give rise to different dynamical regimes. We derive analytically the boundary condition between Josephson oscillations and self-trapping and study numerically the stability of these regimes against perturbations in higher-order OAM modes.

The paper is organized as follows. In Sec. II, we describe the physical system and introduce the few-state model of OAM modes derived from the Gross-Pitaevskii equation (GPE). Section III deals with the stability of the stationary states: after briefly presenting the Bogoliubov analysis, we derive a two-state model, find its critical points, and analyze its associated classical Hamiltonian. The model is then compared against numerical simulations of the complete system of equations derived in Sec. II. Section IV focuses on the dynamical regimes of Josephson oscillations and self-trapping: we first study the case of populating a single mode in each ring and then explore the role of higher-order OAM perturbations. Finally, the conclusions are presented in Sec. V.

\*eulalia.nicolau@uab.cat

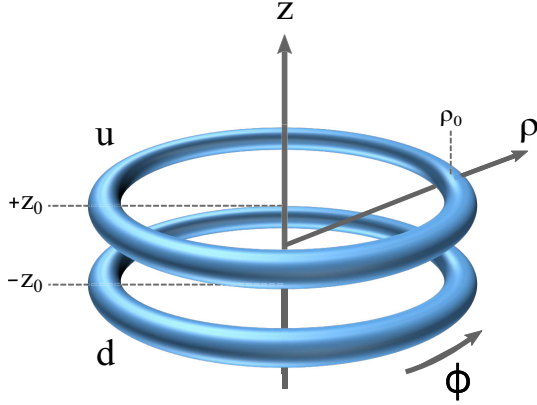


FIG. 1. Schematic of the geometry of the system. The trapping potential consists of two ring traps—up,  $u$ , and down,  $d$ —that are located in the planes  $\pm z_0$ , centered at  $\rho = 0$ , and have radius  $\rho_0$ .

## II. PHYSICAL SYSTEM

The system under consideration is shown in Fig. 1. It consists of two coaxial annular traps around the  $z$  axis separated by a distance  $2z_0$ , where a BEC of  $N$  atoms is trapped. The BEC is described within the mean-field theory by the Gross-Pitaevskii equation, which in cylindrical coordinates reads

$$i\hbar \frac{\partial \Psi(\mathbf{r}, t)}{\partial t} = \left[ \frac{\hbar^2}{2M} \left( -\frac{\partial^2}{\partial \rho^2} - \frac{1}{\rho} \frac{\partial}{\partial \rho} - \frac{\partial^2}{\partial z^2} + \frac{L_z^2}{\hbar^2 \rho^2} \right) + V(\mathbf{r}) + g|\Psi(\mathbf{r}, t)|^2 \right] \Psi(\mathbf{r}, t), \quad (1)$$

where  $V(\mathbf{r})$  is the external potential,  $M$  is the atomic mass,  $L_z = -i\hbar \frac{\partial}{\partial \phi}$  is the  $z$  component of the angular momentum, and  $g = 4\pi\hbar^2 a_s / M$  accounts for the contact interactions characterized by the  $s$ -wave scattering length  $a_s$ . The wave function,  $\Psi(\mathbf{r}, t)$ , is normalized to the total number of particles,  $N$ . Henceforth, we consider exclusively repulsive interactions,  $g > 0$ , and rings with large enough radii so that the term  $\frac{1}{\rho} \frac{\partial}{\partial \rho}$  can be neglected in Eq. (1). The trapping potential in (1) is defined as  $V(\mathbf{r}) = V_z(z) + V_\rho(\rho)$ , where  $V_z$  is a symmetric double-well harmonic potential with minima at  $\pm z_0$ , and  $V_\rho$  is a harmonic radial potential centered at  $\rho_0$ . We assume weak coupling between the rings and that  $V_z$  and  $V_\rho$  are steep enough so that the BEC only presents azimuthal excitations. Then the wave function can be factorized as

$$\Psi(\mathbf{r}, t) = \Psi(\rho) [\Phi^u(z) \chi^u(\phi, t) + \Phi^d(z) \chi^d(\phi, t)], \quad (2)$$

where  $\Psi(\rho)$  is the ground state of the radial harmonic potential and the functions  $\chi^u(\phi, t)$  and  $\chi^d(\phi, t)$  contain the dependence of the BEC wave function with respect to time. The functions  $\Phi^u(z)$  and  $\Phi^d(z)$  are two modes localized in the wells up ( $u$ ) and down ( $d$ ) constructed as a superposition of the ground and first excited stationary solutions of the GPE. The total number of particles in each ring is  $\int d\phi |\chi^{u/d}(\phi, t)|^2 = N^{u/d}(t)$  and the functions  $\Psi(\rho)$ ,  $\Phi^u(z)$ , and  $\Phi^d(z)$  are normalized to 1. The functions  $\chi^u(\phi, t)$  and  $\chi^d(\phi, t)$  for the upper and lower rings can be written as a

linear combination of the angular momentum eigenstates,

$$\chi^{u/d}(\phi, t) = \frac{1}{\sqrt{2\pi}} \sum_{m=-\infty}^{\infty} \alpha_m^{u/d}(t) e^{im\phi}, \quad (3)$$

with amplitudes  $\alpha_m^{u/d}(t)$ . For each eigenstate, the condensate has a quantized angular momentum  $m\hbar$ . The angular mode coefficients are normalized to the number of particles in the  $m$ th angular mode in each ring,  $|\alpha_m^{u/d}(t)|^2 = N_m^{u/d}(t)$ , such that  $N^{u/d}(t) = \sum_m N_m^{u/d}(t)$ . Henceforth, we omit the explicit time dependence in  $\alpha_m^{u/d}(t)$ . The evolution equations for the amplitudes of each OAM mode,  $\alpha_m^{u/d}$ , read [45,46]

$$i \frac{\partial \alpha_m^{u/d}}{\partial \tau} = m^2 \alpha_m^{u/d} - \kappa \alpha_m^{d/u} + \gamma \sum_{m'} \alpha_{m'}^{u/d} (\alpha_{m'}^{u/d})^* \alpha_{m-n+n'}^{u/d}, \quad (4)$$

where  $\tau = \hbar t / (2MR^2)$  is the scaled time,  $\kappa = R^2 \int dz (\Phi^d(z))^* [\frac{\partial^2}{\partial z^2} - \frac{2M}{\hbar^2} V_z] \Phi^u(z)$  is the tunneling rate between the two rings, and  $\gamma = MR^2 g / (\pi \hbar^2) \int d\rho \rho |\Psi(\rho)|^4 \int dz |\Phi^u(z)|^4$  is the interatomic interaction parameter with  $R^{-2} = \int d\rho \rho^{-1} |\Psi(\rho)|^2$ . The first term on the right-hand side in (4) corresponds to the kinetic energy of the  $m$ th mode; the second term, to the tunneling between the two rings, which only couples OAM modes with the same  $m$ ; and the third term is the nonlinear interaction that couples different OAM modes within each ring. The parameters  $\tau$ ,  $\kappa$ ,  $\gamma$  and the other magnitudes appearing in the figures in this work are dimensionless.

## III. STABILITY OF THE STATIONARY STATES

Let us consider that only one OAM mode  $n$  is initially populated in both rings:  $|\alpha_n^{u/d}(\tau = 0)|^2 \neq 0$ ,  $|\alpha_{m \neq n}^{u/d}(\tau = 0)|^2 = 0$ . Then stationary solutions only exist for equal numbers of particles between rings,  $N_n^u = N_n^d = N/2$ , and Eq. (4) simplifies to

$$i\dot{\alpha}_n^{u/d} = n^2 \alpha_n^{u/d} - \kappa \alpha_n^{d/u} + \epsilon \alpha_n^{u/d}, \quad (5)$$

where  $\epsilon = \gamma N/2$  and the overdot indicates the derivative with respect to  $\tau$ . By diagonalizing this system of equations, we find the following symmetric and antisymmetric stationary solutions with energies  $\mu_{\pm}$ :

$$(\alpha_n^u, \alpha_n^d)_s = \sqrt{N} e^{-i\mu_+ \tau} (1, 1), \quad \mu_+ = n^2 + \epsilon - \kappa; \quad (6a)$$

$$(\alpha_n^u, \alpha_n^d)_a = \sqrt{N} e^{-i\mu_- \tau} (1, -1), \quad \mu_- = n^2 + \epsilon + \kappa. \quad (6b)$$

### A. Bogoliubov analysis

In order to study the stability of states (6a) and (6b), we fix  $n = 0$  and add a small-amplitude symmetric perturbation in an arbitrary mode  $m \neq 0$ , of the form

$$\alpha_m^{u/d} = e^{-i\mu_{\pm} \tau} (u_m^{u/d} e^{-i\omega \tau} + (v_m^{u/d})^* e^{i\omega \tau}). \quad (7)$$

By introducing this ansatz together with (6) into (4) and linearizing for small amplitudes of  $u_m^{u/d}$  and  $(v_m^{u/d})^*$ , we obtain the following Bogoliubov–de Gennes equations:

$$\omega u_m^{u/d} = (m^2 - \mu_{\pm} + 2\epsilon) u_m^{u/d} + \epsilon v_{-m}^{u/d} - \kappa u_m^{d/u}, \quad (8a)$$

$$-\omega v_{-m}^{u/d} = (m^2 - \mu_{\pm} + 2\epsilon) v_{-m}^{u/d} + \epsilon u_m^{u/d} - \kappa v_{-m}^{d/u}. \quad (8b)$$

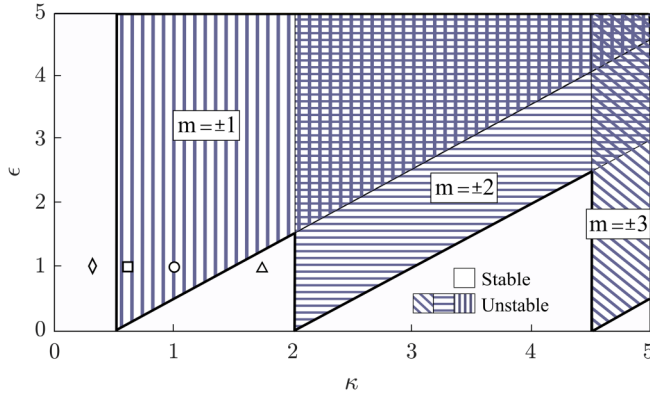


FIG. 2. Real (white) and imaginary (patterned) regions of  $\omega$  for the antisymmetric state with  $n = 0$  and perturbations in the modes  $m = \pm 1, \pm 2, \pm 3$  in the parameter space  $[\kappa, \epsilon]$ . The rhombus, square, circle, and triangle correspond to the parameter values used in Fig. 3, with the circle also being used in Fig. 4.

By diagonalizing (8), one finds that only the antisymmetric state can be unstable against perturbations in higher-order modes. The corresponding excitation branch,  $\omega$ , determines the regions of the parameter space for which the antisymmetric state is unstable [46]:

$$\omega = \sqrt{(m^2 + \epsilon - 2\kappa)^2 - \epsilon^2}. \quad (9)$$

For real values of  $\omega$ , the perturbations, (7), remain periodic and thus bounded, while for imaginary values, the perturbations in mode  $m$  increase exponentially, destabilizing the stationary state. Figure 2 shows the real (white) and imaginary (patterned) regions of  $\omega$  for the stationary state with  $n = 0$  and perturbations in  $m = \pm 1, \pm 2, \pm 3$  as a function of  $\kappa$  and  $\epsilon$ . Interactions increase the instability regions of the antisymmetric state. The spectrum in (9) also holds for stationary solutions with  $n \neq 0$ ; in that case, the perturbation  $m$  is the OAM difference with respect to  $n$ .

## B. Two-state model

The Bogoliubov analysis predicts the stability regions of the stationary solutions in the parameter space. However, it does not describe the dynamics once the stationary state has been destabilized. In order to gain insight into the excitation process, we derive the simplest model that captures these dynamics: a two-state model that includes the antisymmetric stationary state mode and a pair of perturbation modes  $\pm m$ .

We take for simplicity the mode  $n = 0$  for the stationary state, with  $|\alpha_0^u|^2 = N_0^u$  and  $|\alpha_0^d|^2 = N_0^d$ .

We impose the initial condition  $\alpha_0^u = -\alpha_0^d$  and add small-amplitude symmetric perturbations in the high-order modes  $\pm m$  such that  $\delta\alpha_{\pm m}^u = \delta\alpha_{\pm m}^d$ . Due to angular momentum conservation and the fact that the stationary state is in the mode  $n = 0$ , the conditions  $|\alpha_m^u|^2 = |\alpha_{-m}^u|^2$  and  $|\alpha_m^d|^2 = |\alpha_{-m}^d|^2$  are fulfilled. Assuming that the phase difference between the perturbed modes stays approximately constant during the time evolution and that  $|\alpha_{\pm m}^d| \approx |\alpha_{\pm m}^u|$ , we can define  $\alpha_m \equiv \alpha_{\pm m}^u = \alpha_{\pm m}^d$ . We also assume that the initial condition  $\alpha_0^u = -\alpha_0^d \equiv \alpha_0$  is maintained during the temporal evolution, so that we can use  $N^u \approx N^d = N/2$ , where  $N^{u/d} = |\alpha_0^{u/d}|^2 + |\alpha_m^{u/d}|^2 + |\alpha_{-m}^{u/d}|^2$ . Taking these approximations (see Appendix A), the resulting system of equations can be simplified in its matrix form to the following two-state model:

$$i\dot{\alpha}_0 = \left[ \gamma \left( N - |\alpha_0|^2 \left( 1 - 2 \left( \frac{\alpha_m}{\alpha_0} \right)^2 \right) \right) + \kappa \right] \alpha_0, \quad (10a)$$

$$i\dot{\alpha}_m = \left[ \gamma \left( N - |\alpha_m|^2 \left( 1 - \left( \frac{\alpha_0}{\alpha_m} \right)^2 \right) \right) - \kappa + m^2 \right] \alpha_m. \quad (10b)$$

In order to understand the oscillatory dynamics of the system, we define  $\alpha_0 = |\alpha_0|e^{i\phi}$  and  $\alpha_m = |\alpha_m|e^{i\theta}$ . By using particle conservation,  $2|\alpha_0|^2 + 4|\alpha_m|^2 = N$ , and defining the phase difference  $\zeta = \theta - \phi$ , the system reduces to two coupled real equations:

$$|\dot{\alpha}_m|^2 = 2\gamma|\alpha_m|^2 \left( 2|\alpha_m|^2 - \frac{N}{2} \right) \sin 2\zeta, \quad (11a)$$

$$\begin{aligned} \dot{\zeta} = & 2\kappa - m^2 + \gamma \left( 3|\alpha_m|^2 - \frac{N}{2} \right) \\ & + \gamma \left( 4|\alpha_m|^2 - \frac{N}{2} \right) \cos 2\zeta. \end{aligned} \quad (11b)$$

### 1. Critical points

The critical points of this system fulfill  $|\dot{\alpha}_m|^2 = \dot{\zeta} = 0$ . Imposing these conditions in Eqs. (11), we find four critical points and the range of values of  $\kappa$  for which they exist. Table I summarizes the critical points and their existence conditions and Appendix B contains their derivation. By studying the eigenvalues of the Jacobian at the critical points, the first two

TABLE I. Critical points of the two-state model and corresponding existence conditions.

$\zeta$	$ \alpha_m ^2$	$\kappa_{\min}$	$\kappa_{\max}$
$\mathcal{A} = \cos 2\zeta = \frac{-m^2 + 2\kappa - \epsilon}{\epsilon}$	0	$\frac{m^2}{2}$	$\frac{m^2 + 2\epsilon}{2}$
$\mathcal{B} = \cos 2\zeta = \frac{-m^2 + 2\kappa + \frac{\epsilon}{2}}{\epsilon}$	$\frac{N}{4}$	$\frac{m^2 - \frac{3\epsilon}{2}}{2}$	$\frac{m^2 + \frac{\epsilon}{2}}{2}$
$a\pi$	$C = \frac{2\epsilon + m^2 - 2\kappa}{14\epsilon/N}$	$\frac{m^2 - \frac{3\epsilon}{2}}{2}$	$\frac{m^2 + 2\epsilon}{2}$
$(2a + 1)\frac{\pi}{2}$	$D = \frac{2\kappa - m^2}{2\epsilon/N}$	$\frac{m^2}{2}$	$\frac{m^2 + \frac{\epsilon}{2}}{2}$

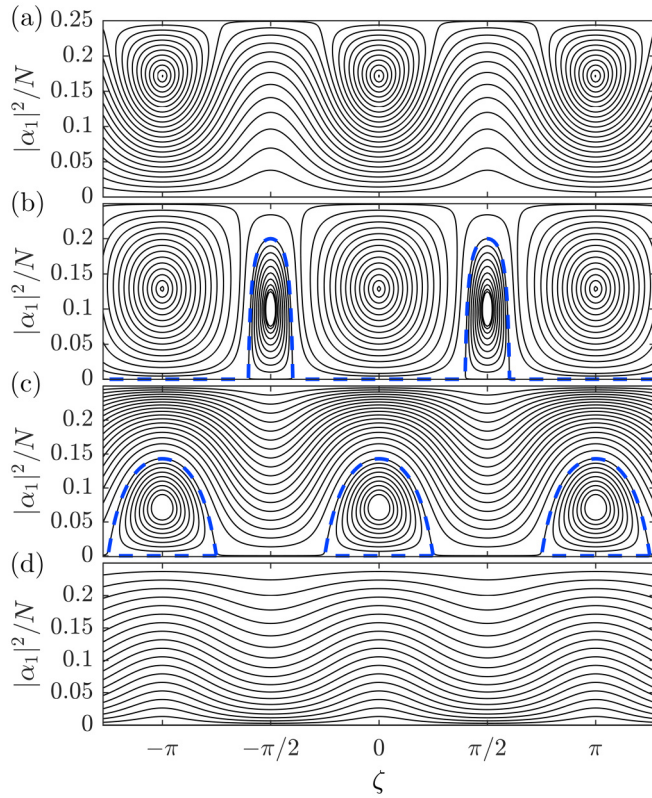


FIG. 3. Lines of constant  $H(|\alpha_m|^2, \zeta)$  for  $m = 1$ ,  $\gamma = 1/2000$ , and  $N = 4000$  (thus,  $\epsilon = 1$ ) and (a)  $\kappa = 0.3$ , (b)  $\kappa = 0.6$ , (c)  $\kappa = 1$ , and (d)  $\kappa = 1.7$ . In dashed blue lines, orbits corresponding to the stationary-state excitations for the unstable cases, (b) and (c). Parameter values of the plots correspond to the rhombus, square, circle, and triangle in Fig. 2, respectively.

solutions can be shown to be saddle points while the other solutions are centers (see Appendix C).

## 2. Two-state model Hamiltonian

Assuming that the variables  $|\alpha_m|^2$  and  $\zeta$  are canonical conjugates, they fulfill  $\partial H/\partial(|\alpha_m|^2) = \zeta$  and  $\partial H/\partial\zeta = -|\alpha_m|^2$ , and thus the corresponding classical Hamiltonian  $H$  reads

$$H(|\alpha_m|^2, \zeta) = |\alpha_m|^2 \left[ 2\kappa - m^2 - \frac{\gamma N}{2} + \frac{3}{2} \gamma |\alpha_m|^2 \right] + \gamma \left( 2|\alpha_m|^2 - \frac{N}{2} \right) \cos 2\zeta. \quad (12)$$

Figure 3 shows lines of constant  $H(|\alpha_m|^2, \zeta)$  for various initial conditions and  $\gamma = 1/2000$ ,  $N = 4000$  (thus,  $\epsilon = 1$ ),  $m = 1$ , and different values of  $\kappa$ . According to the existence conditions of the critical points, Eqs. (B3), (B4), (B6), and (B7), there are four possible types of phase diagrams as a function of the tunneling  $\kappa$ :

(i)  $(m^2 - 3\epsilon/2)/2 < \kappa < m^2/2$ . There are saddle points at  $(\mathcal{B}, |\alpha_m|^2 = N/4)$  and centers at  $(\zeta = a\pi, \mathcal{C})$  [e.g., Fig. 3(a)]. The orbits around the centers are not accessible for the initial conditions  $|\alpha_m|^2/N \simeq 0$  and  $\zeta = 0$ , thus, the stationary state is stable.

(ii)  $m^2/2 < \kappa < (m^2 + \epsilon/2)/2$ . There are saddle points at  $(\mathcal{A}, |\alpha_m|^2 = 0)$  and  $(\mathcal{B}, |\alpha_m|^2 = N/4)$  and centers at  $(\zeta = a\pi, \mathcal{C})$  and  $[\zeta = (2a + 1)\pi/2, \mathcal{D}]$  [e.g., Fig. 3(b)]. Given Eq. (B5), the value of  $|\alpha_m|^2$  corresponding to the centers at  $\zeta = a\pi$  diminishes with the tunneling  $\kappa$ , while the one for the centers at  $\zeta = (2a + 1)\pi/2$  increases with  $\kappa$ . For the values of  $\kappa$  when the  $|\alpha_m|^2$  value of the centers at  $\zeta = a\pi$  is equal to or lower than those of  $\zeta = (2a + 1)\pi/2$ , the system orbits around  $(\zeta = a\pi, \mathcal{C})$ . For lower values of  $\kappa$ , the contrary occurs, and the system performs open orbits around the centers  $[\zeta = (2a + 1)\pi/2, \mathcal{D}]$  [e.g., Fig. 3(b)].

(iii)  $(m^2 + \epsilon/2)/2 < \kappa < (m^2 + 2\epsilon)/2$ . There are saddle points at  $(\mathcal{A}, |\alpha_m|^2 = 0)$  and centers at  $(\zeta = a\pi, \mathcal{C})$  [e.g., Fig. 3(c)], which allows the system to perform orbits around these centers.

(iv) For all other values of  $\kappa$ , i.e.,  $(m^2 + 2\epsilon)/2 < \kappa < (m^2 - 3\epsilon/2)/2$ , there are neither saddle points nor centers [e.g., Fig. 3(d)], such that the stationary state is stable.

Combining all these conditions we find that the antisymmetric stationary state is unstable for  $m^2/2 < \kappa < (m^2 + 2\epsilon)/2$ , which coincides with the stability conditions predicted by the Bogoliubov analysis (see Fig. 2). The Bogoliubov excitations correspond to the open and closed orbits around the centers given the initial conditions  $\zeta = 0$  and  $|\alpha_m|^2/N \simeq 0$ , as the ones shown in dashed blue lines in Figs. 3(b) and 3(c).

The population transfer between the states with  $n = 0$  and the perturbations  $m$  during the excitation is determined by the corresponding orbit. One can find an upper bound to the population transfer,  $|\alpha_m|_{\max}^2/N$ , by considering the initial conditions  $\zeta(\tau = 0) = 0$  and  $|\alpha_m(\tau = 0)|^2/N = 0$ , which correspond to the orbit with  $H(|\alpha_m|^2, \zeta) = 0$ . Taking into account the different possible orbits, either open or closed, and particle conservation in Eq. (12), one reaches

$$\frac{|\alpha_m|_{\max}^2}{N} = \begin{cases} \frac{2\kappa - m^2}{\epsilon}, & \frac{m^2}{2} \leq \kappa \leq \frac{m^2 + \epsilon/4}{2}; \\ \frac{2}{7} \frac{m^2 - 2\kappa + 2\epsilon}{2\epsilon}, & \frac{m^2 + \epsilon/4}{2} \leq \kappa \leq \frac{m^2 + 2\epsilon}{2}. \end{cases} \quad (13)$$

The upper bound of the population transfer increases linearly with the tunneling  $\kappa$  and reaches its maximum for  $\kappa = \frac{\epsilon/4 + m^2}{2}$ , when the centers at  $\zeta = (2a + 1)\pi/2$  and  $\zeta = a\pi$  have the same  $|\alpha_m|^2$ . Then the upper bound of the population transfer decreases linearly with  $\kappa$  down to 0.

For an initial state with  $n \neq 0$ , one observes dynamics analogous to the ones described above, where the pairs of excited modes have an OAM difference  $\pm m$  with respect to  $n$ . For example, for  $\kappa = 1$ ,  $\epsilon = 1$ , and the stationary state with  $n = 0$ , the states that form the excitation are  $m = \pm 1$ , whereas for  $n = 1$ , the excited modes are  $m = 0$  and  $m = 2$ .

## C. Numerical simulations

In this section, we compare numerically the predictions of the two-state model, (10), and the complete system of equations (4), for the stationary state with  $n = 0$ ,  $\kappa = 1$ , and  $\epsilon = 1$  (corresponding to the circle in Fig. 2). Figure 4 shows the time evolution of the populations according to the two-state model (black curve) and by numerical integration of the system of equations (colored curves).

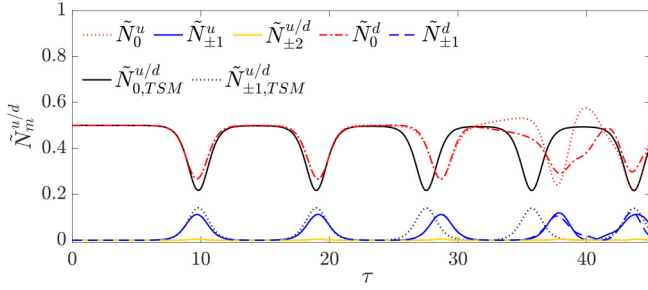


FIG. 4. Temporal evolution of the populations,  $\tilde{N}_m^{u/d} = N_m^{u/d}/N$ , for  $N = 4000$ ,  $\kappa = 1$ , and  $\epsilon = 1$  (circle in Fig. 2) of the two-state model (TSM) with  $m = 1$  (black) and the complete system of equations up to  $m = \pm 15$  (color or gray). Initial conditions:  $\alpha_0^u = -\alpha_0^d = \alpha_0 = \sqrt{N/2}$  with perturbations of order  $\sqrt{N/2} \times 10^{-4}$  [up to  $m = \pm 5$  for the complete system of equations (4)].

For the two-state model, we initially set the amplitudes to  $\alpha_0 = \sqrt{N/2}$  and  $\alpha_1 = \sqrt{N/2} \times 10^{-4}$  in the system of Eqs. (10). The population of the perturbation  $\alpha_1$  increases exponentially, in agreement with Eq. (9) of the Bogoliubov analysis. Then the growth of the perturbation slows down, the population reaches a maximum closely bounded by Eq. (13), and the transfer of population is inverted; the population returns to  $\alpha_0$ . This population transfer pattern is repeated periodically, and for small  $\tau$ , it precisely captures the dynamics predicted by the complete set of equations.

For the full model, we populate equally the  $n = 0$  modes,  $\alpha_0^u = -\alpha_0^d = \sqrt{N/2}$ , and introduce perturbations of order  $\sqrt{N/2} \times 10^{-4}$  for  $m \neq 0$  up to  $m = \pm 5$  in Eq. (4). We include the first  $m = \pm 15$  modes in the simulation, thus truncating the system of equations well above the highest relevant mode. In this case, the excitation is formed by the pair of modes  $m = \pm 1$ , which evolve with the same population within each ring, thus conserving the angular momentum. For long times, the periodic pattern in the evolution of the populations is no longer accurately described by the two-state model since the system does not keep the same population in the  $n = 0$  modes of the two rings. However, the variations in the period and amplitude of the oscillations could be explained using the two-state model, which suggests that the dynamics of the system are highly sensitive to perturbations (see Fig. 3), i.e., a small perturbation can cause the system to change the orbit. Thus, by analogy, the perturbations appearing during the evolution in the full model would lead to oscillations presenting small changes in their period and amplitude. Also, the maximum population that the excitations reach is lower than that of the two-state model due to secondary excitations: the higher-order modes that are also excited modify the dynamics of the main excitation,  $m = \pm 1$ . In this case, the mode  $m = \pm 2$  (yellow line) reaches populations of order  $O(10^{-3})$ , while higher-order modes have smaller contributions.

#### IV. DYNAMICAL REGIMES

Thus far, we have studied the destabilization of the stationary states, which have a single OAM mode  $n$  populated with the same number of particles in both rings. However, when the initial population in each ring is not the same, tunneling

and interactions give rise to different dynamical regimes in the system.

The dynamics of BECs trapped in double-well potentials are known to present either Josephson oscillations or self-trapping, depending on the ratio between the tunneling and the nonlinear interactions [36]. In the Josephson oscillations regime, the population performs complete oscillations between the two wells, while in the self-trapping regime, the population remains mostly trapped in one well. In order to find the self-trapping condition for our system, we initially populate a single mode  $n$  and factorize the amplitudes as

$\alpha_n^{u/d} = \sqrt{N_n^{u/d}} e^{i\beta_n^{u/d}}$ . The system of equations (4) can then be rewritten in terms of the population imbalance,  $z_n = (N_n^u - N_n^d)/N$ , and the phase difference,  $\delta\phi_n = \beta_n^d - \beta_n^u$ , as a set of two coupled equations:

$$\begin{aligned} \dot{z}_n &= -\sqrt{1 - z_n^2} \sin \delta\phi_n, \\ \delta\dot{\phi}_n &= \Lambda z_n + \frac{z_n}{\sqrt{1 - z_n^2}} \cos \delta\phi_n, \end{aligned} \quad (14)$$

where  $\Lambda = \gamma N / (2\kappa) = \epsilon / \kappa$  and  $\tau$  has been scaled to  $2\kappa\tau$ . Assuming that  $z_n$  and  $\delta\phi_n$  are canonically conjugate variables, then  $\partial H / \partial z_n = \delta\dot{\phi}_n$  and  $\partial H / \partial \delta\phi_n = -\dot{z}_n$ , and the corresponding classical Hamiltonian reads

$$H = \frac{1}{2} \Lambda z_n^2 - \cos \delta\phi_n \sqrt{1 - z_n^2}. \quad (15)$$

Note that the Hamiltonian is equal for all  $n$ . Thus, the system presents identical dynamics for all OAM modes. In order to find the boundary between the regimes of self-trapping and Josephson oscillations, we impose  $z_n(\tau) = 0$ , which is only fulfilled in the Josephson oscillations regime. Using energy conservation in (15) and denoting the initial parameters  $z_n(\tau = 0) \equiv z_n(0)$  and  $|\delta\phi_n(\tau = 0)| \equiv \delta\phi_n(0)$ , one reaches

$$\Lambda_c = 2 \left( \frac{\cos \delta\phi_n(0) \sqrt{1 - z_n^2(0)} + 1}{z_n^2(0)} \right), \quad (16)$$

which defines the phase boundary between the two regimes in terms of the initial population imbalance, the phase difference, and the ratio  $\Lambda$ . This condition is a generalization of the one found in [35] for a BEC in a double-well potential. In addition, analogous dynamics are obtained for the total imbalance and phase difference in a system of stacked lattice rings in the deep superfluid limit [16,43]. In this limit, the potential barriers between the sites of the lattices are small enough that the system resembles a couple of free rings. Figure 5 shows the boundary given by (16) for different values of the initial phase difference  $\delta\phi_n(0)$  as a function of  $\Lambda = \epsilon / \kappa$  and the initial population imbalance  $z_n(0)$ . The self-trapping regime occurs for a sufficiently large imbalance and ratio  $\Lambda = \epsilon / \kappa$ . As the phase difference increases from 0 to  $\pi$ , the region of parameters for which self-trapping occurs increases, and as one approaches the limit  $\delta\phi_n(0) \rightarrow \pi$ , the minimum population imbalance to obtain self-trapping approaches  $z_n(0) = 0$ .

The inset in Fig. 5 shows the temporal evolution of the population imbalance,  $z_0$ , for  $z_0(0) = 0.6$ ,  $\delta\phi_n(0) = 0$ , and different values of  $\Lambda$ :  $\Lambda = 4$  [Fig. 5(e)],  $\Lambda = 10$  [Fig. 5(f)], and  $\Lambda = 24$  [Fig. 5(g)]. As the ratio  $\Lambda = \epsilon / \kappa$  increases, the oscillations become anharmonic until the average population

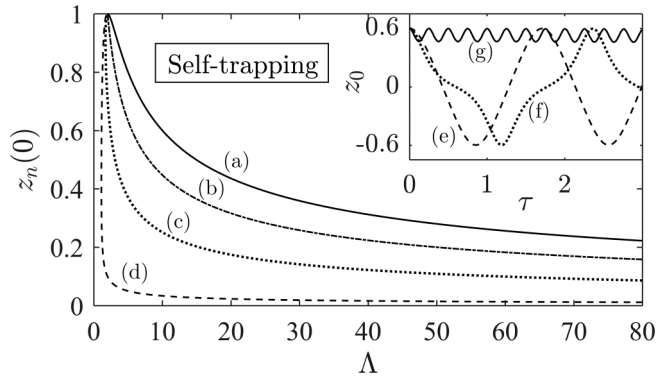


FIG. 5. Boundary between the self-trapping and the Josephson oscillations regimes as predicted by (16) for (a)  $\delta\phi_n(0) = 0$ , (b)  $\delta\phi_n(0) = \pi/2$ , (c)  $\delta\phi_n(0) = 3\pi/4$ , and (d)  $\delta\phi_n(0) \rightarrow \pi$ . Inset: Time evolution of  $z_0$  for  $z_0(0) = 0.6$ ,  $\delta\phi_0(0) = 0$ ,  $N = 4000$ ,  $\kappa = 1$ , and (e)  $\Lambda = 4$ , (f)  $\Lambda = 10$ , and (g)  $\Lambda = 24$ .

imbalance becomes nonzero. If one further increases  $\Lambda$ , the amplitude of the remaining oscillations decreases and they are eventually suppressed; then the population remains at the initial imbalance.

#### Stability of the dynamical regimes

In this section we study numerically the stability of the dynamical regimes, Josephson oscillations, and self-trapping, in the presence of perturbations in higher-order modes. Initially, we populate the mode  $n = 0$  with a certain imbalance  $z_0(0)$  between the rings and a phase difference of  $\pi$  and introduce low-amplitude perturbations in higher-order modes of order  $\sqrt{N/2} \times 10^{-4}$  for  $m \neq 0$  up to  $m = \pm 3$ . Then we also discuss the case where the initial phase difference between the modes with  $n = 0$  is 0.

Figure 6 shows the different dynamics in the parameter space  $[\kappa, \epsilon]$  for  $z_0(0) = 0.1$  [Fig. 6(a)],  $z_0(0) = 0.4$  [Fig. 6(b)], and  $z_0(0) = 0.75$  [Fig. 6(c)]. Black and blue regions indicate stable and unstable self-trapping, respectively, white regions indicate stable Josephson oscillations, and green and yellow regions indicate unstable Josephson oscillations. The simulations run up to  $\tau = 100$ , and the color gradients indicate the decay times. The boundary between Josephson oscillations and self-trapping is not modified by the perturbations, and thus it is determined by Eq. (16) taking  $\delta\phi_0(0) = \pi$ . For a small initial imbalance, Eq. (9) predicts accurately the regions of stability of the dynamical regimes, as the initial state resembles the stationary state [see Figs. 2 and 6(a)]. As the initial imbalance gets larger, the structure of the unstable regions becomes more involved [Figs. 6(b) and 6(c)].

The criteria for classification are the following. The stable regimes are those for which the population of the perturbed modes remains below 0.01. For stable Josephson oscillations, the population imbalance of the main mode becomes 0 at some point during time evolution, whereas in the stable self-trapping regime it does not. The decay time of the unstable regimes is defined as the time for which the total mode populations,  $N_m$ , of the main mode and the perturbation modes cross.

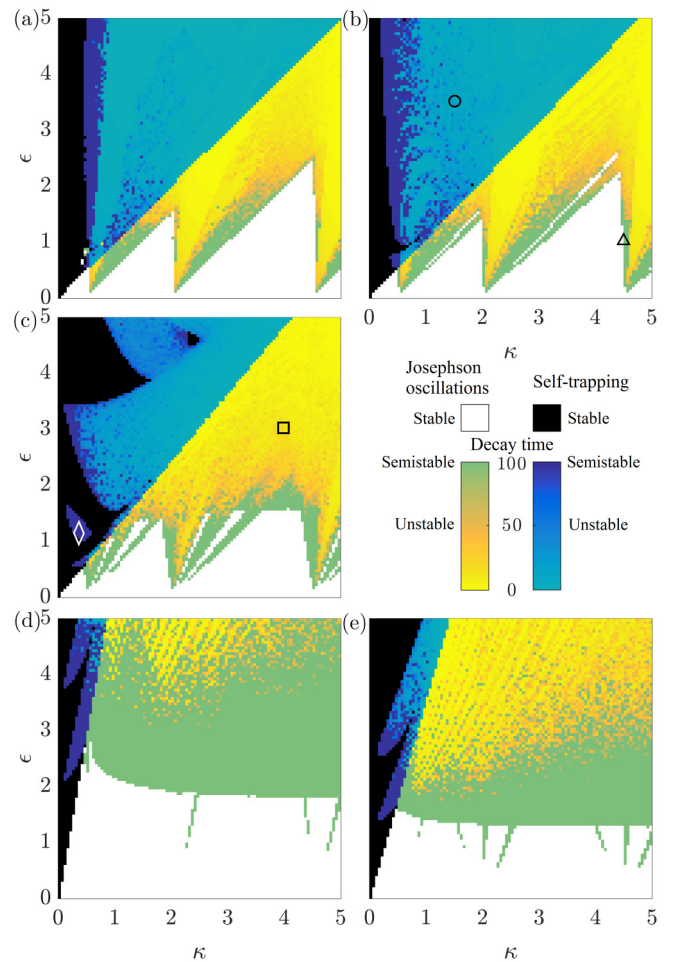


FIG. 6. Dynamical regimes in the parameter space  $[\kappa, \epsilon]$  up to  $\tau = 100$  with  $N = 4000$  for (a)  $z_0(0) = 0.1$ , (b)  $z_0(0) = 0.4$ , (c)  $z_0(0) = 0.75$ , (d)  $z_0(0) = 0.75$ , and (e)  $z_0(0) = 0.9$ . Initial phase difference  $\pi$  for (a)–(c) and 0 for (d) and (e). The square corresponds to the parameters in Fig. 7(a); the circle, to those in Fig. 7(b); the triangle, to those in Fig. 8; and the white rhombus, to those in Fig. 9. For the semistable cases, the dynamics do not decay up to  $\tau = 100$ .

The Josephson oscillations and self-trapping dynamics decay into unstructured oscillations when higher-order modes get excited. The system then remains in a state of nonperiodic oscillations between the two rings that involves several modes. Figure 7 presents examples of these dynamics for unstable Josephson oscillations [Fig. 7(a)] and unstable self-trapping [Fig. 7(b)], corresponding to the square in Fig. 6(c) and the circle in Fig. 6(b), respectively.

Close to the boundary between the stable and the unstable regimes, the system presents semistable Josephson oscillations and self-trapping. In these cases, the population of a single excited mode  $\pm m$  increases and decays periodically, without destabilizing the dynamics of the main mode,  $n = 0$ . Figures 8(a) and 9(a) show an example of semistable Josephson dynamics and semistable self-trapping dynamics, respectively. Figures 8(b) and 9(b) show the corresponding total mode populations  $\tilde{N}_m^u + \tilde{N}_m^d = (N_m^u + N_m^d)/N$ , which present a pattern analogous to those shown by Bogoliubov excitations of the stationary state (see Fig. 4). Therefore, the semistable

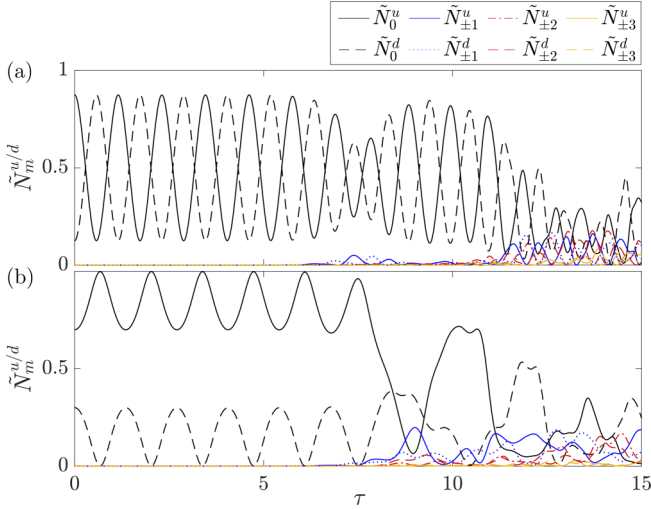


FIG. 7. Temporal evolution of the populations,  $\tilde{N}_m^{u/d} = N_m^{u/d}/N$  with  $N = 4000$ , for unstable Josephson oscillations (a)  $\kappa = 4$ ,  $\epsilon = 3$ ,  $z_0(0) = 0.75$  [square in Fig. 6(c)] and unstable self-trapping (b)  $\kappa = 1.5$ ,  $\epsilon = 3.5$ ,  $z_0(0) = 0.4$  [circle in Fig. 6(b)]. The modes that grow from  $\tau = 5$  onwards include  $m = \pm 1, \pm 2, \pm 3$ .

dynamics can be understood as Bogoliubov excitations of the dynamical states modulated by tunneling.

Figures 6(d) and 6(e) show the different dynamics in the parameter space  $[\kappa, \epsilon]$  for initial imbalance  $z_0(0) = 0.75$  and  $z_0(0) = 0.9$ , respectively. For these cases, the initial phase difference between the modes with  $n = 0$  is 0. In these cases the boundary between Josephson oscillations and self-trapping is given by Eq. (16) taking  $\delta\phi_0(0) = 0$  (see Fig. 5). Consequently, the Josephson oscillations regimes are much larger than those with an initial phase difference equal to  $\pi$  [see Figs. 6(a)–6(c)]. As the initial phase difference is 0, which corresponds to the symmetric state in the stationary case, there is no mechanism of Bogoliubov destabilization and the unstable regimes do not resemble the spectrum in

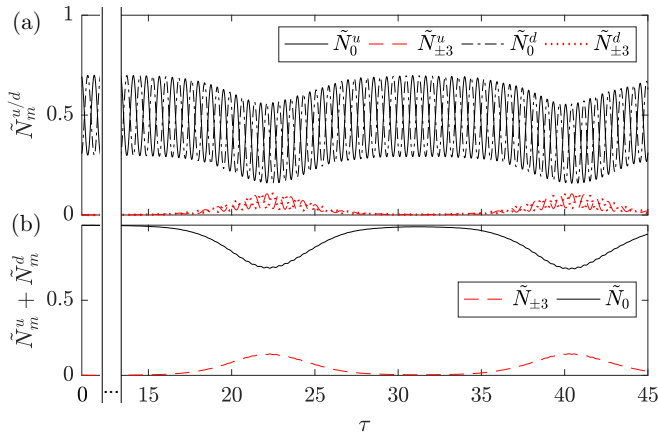


FIG. 8. Temporal evolution of semistable Josephson oscillations for  $\kappa = 4.5$ ,  $\epsilon = 1$ ,  $N = 4000$ , and  $z_0(0) = 0.4$  [triangle in Fig. 6(b)] for (a) the populations in each mode and ring,  $\tilde{N}_m^{u/d} = N_m^{u/d}/N$ , and (b) the total mode populations,  $\tilde{N}_m^u + \tilde{N}_m^d$ . Note that the time axis has a gap between  $\tau = 0$  and  $\tau = 15$  to show the relevant dynamics.

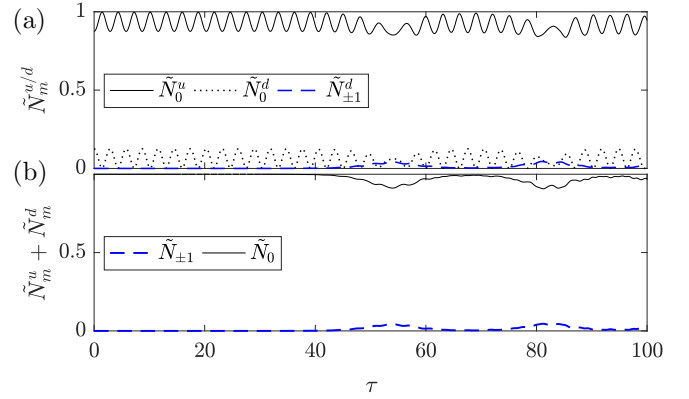


FIG. 9. Temporal evolution of semistable self-trapping for  $\kappa = 0.35$ ,  $\epsilon = 1.25$ ,  $N = 4000$ , and  $z_0(0) = 0.75$  [rhombus in Fig. 6(c)] for (a) the populations in each mode and ring,  $\tilde{N}_m^{u/d} = N_m^{u/d}/N$ , and (b) the total mode populations,  $\tilde{N}_m^u + \tilde{N}_m^d$ . The populations of the modes  $\alpha_{\pm 1}^u$  remain below 0.01.

Fig. 2. Instead, there is an interactions threshold that depends mainly on the imbalance above which the Josephson oscillations become unstable. For an initial imbalance  $z_0(0) = 0.4$ , both regimes are stable and the Josephson oscillations regime occupies the vast majority of the considered parameter space.

The time scales considered in this section, which go up to  $\tau = 100$ , reach the order of 8 s for  $^{87}\text{Rb}$ , a ring radius of  $\rho_0 = 5 \times 10^{-6}$  m, and an oscillator length of the harmonic potentials  $a = 1 \times 10^{-6}$  m. Within a time scale up to  $\tau = 10$ , which corresponds to 0.8 s, one would observe several Josephson oscillations, as shown in Figs. 7(a) and 8(a). Therefore, the described dynamics are within reach in state-of-the-art experiments.

## V. CONCLUSIONS

In this work, we have investigated a Bose-Einstein condensate with repulsive interactions trapped in two rings in a stack configuration. The stability and dynamics of the BEC have been studied within mean-field theory and in terms of its OAM modes. For the case of a single mode equally populated in both rings and including small perturbations in other modes, we have derived a two-state model that predicts the regions of the parameter space supporting stable stationary states. This model also describes the dynamics of the system after destabilization and characterizes accurately the features of the excitations. The analytical results of the two-state model have been contrasted with the numerical integration of the full model, finding a good qualitative and quantitative agreement.

Also, we have analyzed the dynamics of the system when a single OAM mode is populated with an arbitrary population imbalance between the two rings: the dynamical regimes of Josephson oscillations and self-trapping. The boundary condition between the two regimes has been analytically derived in terms of the population imbalance and the corresponding phase difference. We have found that the dynamics are equal for all OAM modes and resemble the dynamics of a double-well system. By numerical analysis, we have characterized these dynamical regimes against perturbations in higher-order OAM modes.

## ACKNOWLEDGMENTS

We are grateful to Armengol Gasull for fruitful discussions. Also, E.N., V.A., and J.M. acknowledge support from the Ministerio de Economía y Competitividad (MINECO; Contract No. FIS2017-86530-P) and the Gen-

eralitat de Catalunya (Contract No. SGR2017-1646). E.N. acknowledges financial support from MINECO through Grant No. PRE2018-085815. B.J.D. acknowledges support from MINECO (Contract No. FIS2017-87534-P) and the Generalitat de Catalunya (Contract No. 2017SGR-533).

## APPENDIX A: TWO-STATE MODEL DERIVATION

In order to derive the two-state model in Sec. III B, Eq. (10), we take for simplicity the mode  $n = 0$  for the stationary state, with  $|\alpha_0^u|^2 = N_0^u$  and  $|\alpha_0^d|^2 = N_0^d$ . Then the system of equations (4) reduces to a set of six equations that can be expressed in matrix form as

$$i \begin{pmatrix} \dot{\alpha}_0^u \\ \dot{\alpha}_m^u \\ \dot{\alpha}_{-m}^u \\ \dot{\alpha}_0^d \\ \dot{\alpha}_m^d \\ \dot{\alpha}_{-m}^d \end{pmatrix} = \hat{A} \cdot \begin{pmatrix} \alpha_0^u \\ \alpha_m^u \\ \alpha_{-m}^u \\ \alpha_0^d \\ \alpha_m^d \\ \alpha_{-m}^d \end{pmatrix}, \quad (\text{A1})$$

where the matrix  $\hat{A}$  reads

$$\begin{pmatrix} \gamma(2N^u - |\alpha_0^u|^2) & \gamma\alpha_{-m}^u(\alpha_0^u)^* & \gamma\alpha_m^u(\alpha_0^u)^* & -\kappa & 0 & 0 \\ \gamma\alpha_0^u(\alpha_{-m}^u)^* & m^2 + \gamma(2N^u - |\alpha_m^u|^2) & 0 & 0 & -\kappa & 0 \\ \gamma\alpha_0^u(\alpha_m^u)^* & 0 & m^2 + \gamma(2N^u - |\alpha_{-m}^u|^2) & 0 & 0 & -\kappa \\ -\kappa & 0 & 0 & \gamma(2N^d - |\alpha_0^d|^2) & \gamma\alpha_{-m}^d(\alpha_0^d)^* & \gamma\alpha_m^d(\alpha_0^d)^* \\ 0 & -\kappa & 0 & \gamma\alpha_0^d(\alpha_{-m}^d)^* & m^2 + \gamma(2N^d - |\alpha_m^d|^2) & 0 \\ 0 & 0 & -\kappa & \gamma\alpha_0^d(\alpha_m^d)^* & 0 & m^2 + \gamma(2N^d - |\alpha_{-m}^d|^2) \end{pmatrix}, \quad (\text{A2})$$

with  $N^{u/d} = |\alpha_0^{u/d}|^2 + |\alpha_m^{u/d}|^2 + |\alpha_{-m}^{u/d}|^2$  being the total number of particles in the  $u$  and  $d$  rings. We impose the initial condition  $\alpha_0^u = -\alpha_0^d$  and add small-amplitude symmetric perturbations in the high-order modes  $\pm m$  such that  $\delta\alpha_{\pm m}^u = \delta\alpha_{\pm m}^d$ . Due to angular momentum conservation and the fact that the stationary state is in the mode  $n = 0$ , the conditions  $|\alpha_m^u|^2 = |\alpha_{-m}^u|^2$  and  $|\alpha_m^d|^2 = |\alpha_{-m}^d|^2$  are fulfilled. Assuming that the phase difference between the perturbed modes stays approximately constant during the time evolution and that  $|\alpha_{\pm m}^d| \approx |\alpha_{\pm m}^u|$ , we can define  $\alpha_m \equiv \alpha_{\pm m}^u = \alpha_{\pm m}^d$ . We also assume that the initial condition  $\alpha_0^u = -\alpha_0^d$  is maintained during the temporal evolution, so that we can also use  $N^u \approx N^d = N/2$ . Applying all these conditions, expression (A1) can be simplified to a set of three equations for  $\alpha_0^u$ ,  $\alpha_m$ , and  $\alpha_0^d$ , which in matrix form reads

$$i \begin{pmatrix} \dot{\alpha}_0^u \\ \dot{\alpha}_m \\ \dot{\alpha}_0^d \end{pmatrix} = \begin{pmatrix} \gamma(N - |\alpha_0^u|^2(1 - 2(\frac{\alpha_m}{\alpha_0^u})^2)) & 0 & -\kappa \\ 0 & -\kappa + m^2 + \gamma(N - |\alpha_m|^2(1 - (\frac{\alpha_m}{\alpha_m})^2)) & 0 \\ -\kappa & 0 & \gamma(N - |\alpha_0^d|^2(1 - 2(\frac{\alpha_m}{\alpha_0^d})^2)) \end{pmatrix} \begin{pmatrix} \alpha_0^u \\ \alpha_m \\ \alpha_0^d \end{pmatrix}. \quad (\text{A3})$$

This system can be reduced further by noting that the first and last diagonal elements are equal. Then, defining  $\alpha_0 \equiv \alpha_0^u$ , we obtain the following two-state model:

$$i \begin{pmatrix} \dot{\alpha}_0 \\ \dot{\alpha}_m \end{pmatrix} = \begin{pmatrix} \gamma(N - |\alpha_0|^2(1 - 2(\frac{\alpha_m}{\alpha_0})^2)) + \kappa & 0 \\ 0 & -\kappa + m^2 + \gamma(N - |\alpha_m|^2(1 - (\frac{\alpha_m}{\alpha_m})^2)) \end{pmatrix} \begin{pmatrix} \alpha_0 \\ \alpha_m \end{pmatrix}. \quad (\text{A4})$$

## APPENDIX B: CRITICAL POINTS DERIVATION

The critical points of the two-state model, discussed in Sec. III B, fulfill  $|\dot{\alpha}_m|^2 = \dot{\zeta} = 0$ . Imposing  $|\dot{\alpha}_m|^2 = 0$  in Eq. (11a), we find

$$|\alpha_m|^2 = 0, \quad |\alpha_m|^2 = \frac{N}{4}, \quad \sin 2\zeta = 0, \quad (\text{B1})$$



where the first two trivial solutions correspond to the minimum and maximum values of  $|\alpha_m|^2$  that are due to particle conservation. The critical points can then be found by imposing  $\dot{\zeta} = 0$  in Eq. (11b). For the trivial cases, the critical points are

$$\left( \cos 2\zeta = \frac{2\kappa - m^2 - \epsilon}{\epsilon} \equiv \mathcal{A}, |\alpha_m|^2 = 0 \right), \quad (\text{B2a})$$

$$\left( \cos 2\zeta = \frac{m^2 - 2\kappa - \epsilon/2}{\epsilon} \equiv \mathcal{B}, |\alpha_m|^2 = \frac{N}{4} \right). \quad (\text{B2b})$$

Due to the boundedness of the cosine in (B2a), the solution with  $|\alpha_m|^2 = 0$  exists if

$$\frac{m^2}{2} \leq \kappa \leq \frac{m^2 + 2\epsilon}{2}, \quad (\text{B3})$$

and similarly, the solution with  $|\alpha_m|^2 = N/4$ , Eq. (B2b), exists if

$$\frac{m^2 - 3\epsilon/2}{2} \leq \kappa \leq \frac{m^2 + \epsilon/2}{2}. \quad (\text{B4})$$

By studying the eigenvalues of the Jacobian at the critical points, these trivial solutions can be shown to be saddle points (see Appendix C).

For the nontrivial solution, for which  $|\alpha_m|^2$  takes values different from 0 or  $N/4$ , the critical points are

$$\left( \zeta = a\pi, \quad |\alpha_m|^2 = \frac{m^2 - 2\kappa + 2\epsilon}{14\epsilon/N} \equiv \mathcal{C} \right), \quad (\text{B5a})$$

$$\left( \zeta = (2a + 1)\frac{\pi}{2}, \quad |\alpha_m|^2 = \frac{2\kappa - m^2}{2\epsilon/N} \equiv \mathcal{D} \right), \quad (\text{B5b})$$

where  $a \in \mathbb{Z}$ . Taking into account the minimum and maximum values of  $|\alpha_m|^2$  due to particle conservation, the solutions with  $\zeta = a\pi$  exist if

$$\frac{m^2 - 3\epsilon/2}{2} \leq \kappa \leq \frac{m^2 + 2\epsilon}{2}, \quad (\text{B6})$$

whereas those with  $\zeta = (2a + 1)\pi/2$  exist if

$$\frac{m^2}{2} \leq \kappa \leq \frac{m^2 + \epsilon/2}{2}. \quad (\text{B7})$$

Note that the second set of solutions, Eq. (B5b), has a more restrictive condition than the first, Eq. (B5a). Similarly as before, these solutions can be shown to be centers, with the trajectories orbiting around them (see Appendix C).

### APPENDIX C: PROPERTIES OF THE CRITICAL POINTS

For the two-state model derived in Sec. III B, the behavior of the system around the critical points can be obtained by studying the eigenvalues of the Jacobian at the critical points. The Jacobian reads

$$DF = \begin{pmatrix} \frac{\partial(|\alpha_m|^2)}{\partial(|\alpha_m|^2)} & \frac{\partial\dot{\zeta}}{\partial(|\alpha_m|^2)} \\ \frac{\partial(|\alpha_m|^2)}{\partial\zeta} & \frac{\partial\dot{\zeta}}{\partial\zeta} \end{pmatrix} = \begin{pmatrix} \gamma(8|\alpha_m|^2 - N) \sin 2\zeta & 3\gamma + 4\gamma \cos 2\zeta \\ 4\gamma|\alpha_m|^2(2|\alpha_m|^2 - \frac{N}{2}) \cos 2\zeta & -2\gamma(4\gamma|\alpha_m|^2 - \frac{N}{2}) \sin 2\zeta \end{pmatrix}. \quad (\text{C1})$$

For the critical point  $(\mathcal{A}, |\alpha_m|^2 = 0)$ ,

$$DF(\mathcal{A}, |\alpha_m|^2 = 0) = \begin{pmatrix} -\gamma N \sin 2\zeta & 3\gamma + 4\gamma \cos 2\zeta \\ 0 & \gamma N \sin 2\zeta \end{pmatrix}. \quad (\text{C2})$$

The corresponding eigenvalues are real and have opposite sign,  $\lambda = \pm\gamma N \sin 2\zeta$ , thus, the critical point is a saddle point. For the limiting values of  $\kappa$  in the existence condition of the critical point, Eq. (B3),  $m^2/2$  and  $(m^2 + 2\epsilon)/2$ ,  $\zeta$  takes the values  $(2a + 1)\pi/2$  and  $a\pi$ , respectively. In those cases, the eigenvalues become 0 and the behavior around the critical point cannot be inferred from this method.

Similarly, for  $(\mathcal{B}, |\alpha_m|^2 = N/4)$ ,

$$DF\left(\mathcal{B}, |\alpha_m|^2 = \frac{N}{4}\right) = \begin{pmatrix} \gamma N \sin 2\zeta & 3\gamma + 4\gamma \cos 2\zeta \\ 0 & -\gamma N \sin 2\zeta \end{pmatrix}, \quad (\text{C3})$$

and the eigenvalues are real numbers of opposite sign,  $\lambda = \pm\gamma N \sin 2\zeta$ . Thus, this critical point is a saddle point, except for the limiting cases in Eq. (B4).

For the critical point ( $\zeta = a\pi, \mathcal{C}$ ),

$$DF(\zeta = a\pi, \mathcal{C}) = \begin{pmatrix} 0 & 7\gamma \\ 4\gamma|\alpha_m|^2(2|\alpha_m|^2 - \frac{N}{2}) & 0 \end{pmatrix}, \quad (\text{C4})$$

and the eigenvalues are

$$\lambda = \pm\sqrt{28\gamma^2|\alpha_m|^2\left(2|\alpha_m|^2 - \frac{N}{2}\right)}. \quad (\text{C5})$$

Using the  $|\alpha_m|^2$  value of the critical point in Eq. (B5a), these eigenvalues are imaginary, thus the stationary point is a center, and the trajectories precede around it. For the limiting values of  $\kappa$  in Eq. (B6),  $(m^2 - 3\epsilon/2)/2$  and  $(m^2 + 2\epsilon)/2$ ,  $|\alpha_m|^2$  becomes  $N/4$  and 0, respectively, in which case both eigenvalues are 0 and the behavior around the critical point cannot be determined.

For ( $\zeta = (2a + 1)\frac{\pi}{2}, \mathcal{D}$ ),

$$DF\left(\zeta = (2a + 1)\frac{\pi}{2}, \mathcal{D}\right) = \begin{pmatrix} 0 & -\gamma \\ -4\gamma|\alpha_m|^2(2|\alpha_m|^2 - \frac{N}{2}) & 0 \end{pmatrix}, \quad (\text{C6})$$

with eigenvalues

$$\lambda = \pm\sqrt{4\gamma^2|\alpha_m|^2\left(2|\alpha_m|^2 - \frac{N}{2}\right)}. \quad (\text{C7})$$

As before, these stationary points are centers, and the trajectories precede around them, except for the limiting values of  $\kappa$  in Eq. (B7).

- 
- [1] B. T. Seaman, M. Krämer, D. Z. Anderson, and M. J. Holland, *Phys. Rev. A* **75**, 023615 (2007).
- [2] L. Amico, G. Birkel, M. Boshier, and L.-C. Kwek, *New J. Phys.* **19**, 020201 (2017).
- [3] B. E. Sherlock, M. Gildemeister, E. Owen, E. Nugent, and C. J. Foot, *Phys. Rev. A* **83**, 043408 (2011).
- [4] A. S. Arnold, *Opt. Lett.* **37**, 2505 (2012).
- [5] G. Pelegrí, J. Mompart, and V. Ahufinger, *New J. Phys.* **20**, 103001 (2018).
- [6] B. Barrett, R. Geiger, I. Dutta, M. Meunier, B. Canuel, A. Gauguier, P. Bouyer, and A. Landragin, *C.R. Phys.* **15**, 875 (2014).
- [7] J. L. Helm, S. L. Cornish, and S. A. Gardiner, *Phys. Rev. Lett.* **114**, 134101 (2015).
- [8] F. I. Moxley, J. P. Dowling, W. Dai, and T. Byrnes, *Phys. Rev. A* **93**, 053603 (2016).
- [9] S. P. Nolan, J. Sabbatini, M. W. J. Bromley, M. J. Davis, and S. A. Haine, *Phys. Rev. A* **93**, 023616 (2016).
- [10] P. Navez, S. Pandey, H. Mas, K. Poullos, T. Fernholz, and W. von Klitzing, *New J. Phys.* **18**, 075014 (2016).
- [11] S. Safaei, L.-C. Kwek, R. Dumke, and L. Amico, *Phys. Rev. A* **100**, 013621 (2019).
- [12] B. P. Anderson, K. Dholakia, and E. M. Wright, *Phys. Rev. A* **67**, 033601 (2003).
- [13] A. Ramanathan, K. C. Wright, S. R. Muniz, M. Zelan, W. T. Hill, C. J. Lobb, K. Helmerston, W. D. Phillips, and G. K. Campbell, *Phys. Rev. Lett.* **106**, 130401 (2011).
- [14] K. C. Wright, R. B. Blakestad, C. J. Lobb, W. D. Phillips, and G. K. Campbell, *Phys. Rev. Lett.* **110**, 025302 (2013).
- [15] C. Ryu, P. W. Blackburn, A. A. Blinova, and M. G. Boshier, *Phys. Rev. Lett.* **111**, 205301 (2013).
- [16] L. Amico, D. Aghamalyan, F. Auzsztol, H. Crepez, R. Dumke, and L. C. Kwek, *Sci. Rep.* **4**, 4298 (2015).
- [17] S. Eckel, J. G. Lee, F. Jendrzejewski, N. Murray, C. W. Clark, C. J. Lobb, W. D. Phillips, M. Edwards, and G. K. Campbell, *Nature* **506**, 200 (2014).
- [18] S. Eckel, F. Jendrzejewski, A. Kumar, C. J. Lobb, and G. K. Campbell, *Phys. Rev. X* **4**, 031052 (2014).
- [19] F. Jendrzejewski, S. Eckel, N. Murray, C. Lanier, M. Edwards, C. J. Lobb, and G. K. Campbell, *Phys. Rev. Lett.* **113**, 045305 (2014).
- [20] Y.-H. Wang, A. Kumar, F. Jendrzejewski, R. M. Wilson, M. Edwards, S. Eckel, G. K. Campbell, and C. W. Clark, *New J. Phys.* **17**, 125012 (2015).
- [21] S. Beattie, S. Moulder, R. J. Fletcher, and Z. Hadzibabic, *Phys. Rev. Lett.* **110**, 025301 (2013).
- [22] L. Corman, L. Chomaz, T. Bienaimé, R. Desbuquois, C. Weitenberg, S. Nascimbène, J. Dalibard, and J. Beugnon, *Phys. Rev. Lett.* **113**, 135302 (2014).
- [23] M. F. Andersen, C. Ryu, P. Cladé, V. Natarajan, A. Vaziri, K. Helmerston, and W. D. Phillips, *Phys. Rev. Lett.* **97**, 170406 (2006).
- [24] S. Gupta, K. W. Murch, K. L. Moore, T. P. Purdy, and D. M. Stamper-Kurn, *Phys. Rev. Lett.* **95**, 143201 (2005).
- [25] O. Morizot, Y. Colombe, V. Lorent, H. Perrin, and B. M. Garraway, *Phys. Rev. A* **74**, 023617 (2006).
- [26] C. Ryu, M. F. Andersen, P. Cladé, V. Natarajan, K. Helmerston, and W. D. Phillips, *Phys. Rev. Lett.* **99**, 260401 (2007).
- [27] A. Turpin, J. Polo, Y. V. Loiko, J. Küber, F. Schmaltz, T. K. Kalkandjiev, V. Ahufinger, G. Birkel, and J. Mompart, *Opt. Express* **23**, 1638 (2015).

- [28] F. Moscatelli, C. Sackett, S. Du, and E. Oh, *Phys. Rev. A* **76**, 043404 (2007).
- [29] E. M. Wright, J. Arlt, and K. Dholakia, *Phys. Rev. A* **63**, 013608 (2000).
- [30] T. A. Bell, J. A. Glidden, L. Humbert, M. W. Bromley, S. A. Haine, M. J. Davis, T. W. Neely, M. A. Baker, and H. Rubinsztein-Dunlop, *New J. Phys.* **18**, 035003 (2016).
- [31] S. K. Schnelle, E. D. van Ooijen, M. J. Davis, N. R. Heckenberg, and H. Rubinsztein-Dunlop, *Opt. Express* **16**, 1405 (2008).
- [32] K. Henderson, C. Ryu, C. MacCormick, and M. G. Boshier, *New J. Phys.* **11**, 043030 (2009).
- [33] B. Josephson, *Phys. Lett.* **1**, 251 (1962).
- [34] P. W. Anderson and J. M. Rowell, *Phys. Rev. Lett.* **10**, 230 (1963).
- [35] A. Smerzi, S. Fantoni, S. Giovanazzi, and R. Shenoy, *Phys. Rev. Lett.* **79**, 4950 (1997).
- [36] M. Albiez, R. Gati, J. Fölling, S. Hunsmann, M. Cristiani, and M. K. Oberthaler, *Phys. Rev. Lett.* **95**, 010402 (2005).
- [37] Y. Shin, G.-B. Jo, M. Saba, T. A. Pasquini, W. Ketterle, and D. E. Pritchard, *Phys. Rev. Lett.* **95**, 170402 (2005).
- [38] S. Levy, E. Lahoud, I. Shomroni, and J. Steinhauer, *Nature* **449**, 579 (2007).
- [39] T. Schumm, S. Hofferberth, L. M. Andersson, S. Wildermuth, S. Groth, I. Bar-Joseph, J. Schmiedmayer, and P. Krüger, *Nat. Phys.* **1**, 57 (2005).
- [40] B. V. Hall, S. Whitlock, R. Anderson, P. Hannaford, and A. I. Sidorov, *Phys. Rev. Lett.* **98**, 030402 (2007).
- [41] G.-B. Jo, Y. Shin, S. Will, T. A. Pasquini, M. Saba, W. Ketterle, D. E. Pritchard, M. Vengalattore, and M. Prentiss, *Phys. Rev. Lett.* **98**, 030407 (2007).
- [42] J. Estève, C. Gross, A. Weller, S. Giovanazzi, and M. K. Oberthaler, *Nature* **455**, 1216 (2008).
- [43] D. Aghamalyan, L. Amico, and L. C. Kwek, *Phys. Rev. A* **88**, 063627 (2013).
- [44] A. Escrivà, A. M. Mateo, M. Guilleumas, and B. Juliá-Díaz, *Phys. Rev. A* **100**, 063621 (2019).
- [45] I. Lesanovsky and W. von Klitzing, *Phys. Rev. Lett.* **98**, 050401 (2007).
- [46] J. Brand, T. J. Haigh, and U. Zülicke, *Phys. Rev. A* **81**, 025602 (2010).
- [47] N. V. Hung, K. Zegadlo, A. Ramaniuk, V. V. Konotop, and M. Trippenbach, *Sci. Rep.* **7**, 4089 (2017).
- [48] A. Richaud and V. Penna, *Phys. Rev. A* **96**, 013620 (2017).
- [49] A. Ramaniuk, N. Hung, M. Giersig, K. Kempa, V. Konotop, and M. Trippenbach, *Symmetry* **10**, 195 (2018).
- [50] K. Zegadlo, H. V. Nguyen, V. V. Konotop, J. Zakrzewski, and M. Trippenbach, *Nonlin. Dynam.* **97**, 559 (2019).
- [51] A. Oliinyk, I. Yatsuta, B. Malomed, and A. Yakimenko, *Symmetry* **11**, 1312 (2019).
- [52] A. Oliinyk, A. Yakimenko, and B. Malomed, *J. Phys. B: At. Mol. Opt. Phys.* **52**, 225301 (2019).
- [53] A. Oliinyk, B. Malomed, and A. Yakimenko, *Commun. Nonlin. Sci. Numer. Simul.* **83**, 105113 (2020).
- [54] X.-F. Zhang, R.-F. Dong, T. Liu, W. M. Liu, and S.-G. Zhang, *Phys. Rev. A* **86**, 063628 (2012).
- [55] J. Polo, A. Benseny, T. Busch, V. Ahufinger, and J. Mompert, *New J. Phys.* **18**, 015010 (2016).
- [56] J. Polo, J. Mompert, and V. Ahufinger, *Phys. Rev. A* **93**, 033613 (2016).
- [57] T. Bland, Q. Marolleau, P. Comaron, B. Malomed, and N. Proukakis, *J. Phys. B: At. Mol. Opt. Phys.* **53**, 115301 (2020).